Computation of the Equivalent Macroscopic Permeability Tensor of Discrete Networks with Heterogeneous Segment Length

D. Bauer, Ph.D.[1]; L. Talon, Ph.D.[2]; and A. Ehrlacher[3]

Abstract: Flow in discrete networks can be observed in biological, geological, or technical systems. Often, the number of individual segments is very large. Therefore, discrete pressure and flow calculation in each single segment becomes very time consuming, and a continuum model becomes attractive. We apply a global upscaling method based on a spatial average to investigate a porous media network model with heterogeneous pore length distribution. For this purpose, the porous media was modeled by triangular networks. For such networks, we characterize the representative elementary volume (REV) size and show that using window sizes smaller than the REV requires an heterogeneous Darcian description. We find that the permeability has to be distributed according to a log-Gaussian distribution with variance and correlation length depending on the window size and the porous microstructure. Finally, we apply the procedure to an anisotropic regular network for which an analytical solution can be found and show that using this method leads to the correct analytical behavior.

DOI: 10.1061/(ASCE)0733-9429(2008)134:6(784)

CE Database subject headings: Porous media; Hydraulic networks; Heterogeneity.

Introduction

Very dense, geometrically complex networks can be found in geological, biological, or technical systems. Common examples are blood flow at the capillary level or water flow in highly fractured rocks. In particular, intergranular microcracks due to tension in the rock build very dense fracture networks. Often, in these cases the fracture aperture is very small in comparison to its length. Consequently, the heterogeneity of these rock types is generally due to the heterogeneous length distribution. Flow and pressure computation in these rock types, considering all fractures, is very time consuming. Therefore, it may be worthwhile to develop a continuum description of the discrete network that describes effectively the underlying network geometry. The main objective of this paper is to characterize a porous medium described by a discrete network with heterogeneous pore length distribution, assuming a Poiseuille flow on the level of the individual segment of the network. Toward this goal we propose an upscaling method based on global boundary conditions and a spatial average.

[1]Laboratoire d'Analyse des Matériaux et Identification, Ecole Nationale des Ponts et Chaussées, 6 et 8 Ave. B.Pascal, Cité Descartes, 77455 Marne La Vallée, Cedex 2, France (corresponding author). E-mail: bauer@fast.u.psud.fr

[2]Laboratoire FAST, UMR CNRS 7608, Univ. Paris VI et Paris XI, Bâtiment 502, Campus Universitaire, 91405 Orsay Cedex, France.

[3]Professor, Laboratoire d'Analyse des Matériaux et Identification, Ecole Nationale des Ponts et Chaussées, 6 et 8 Ave. B. Pascal, Cité Descartes, 77455 Marne La Vallée, Cedex 2, France.

Note. Discussion open until November 1, 2008. Separate discussions must be submitted for individual papers. To extend the closing date by one month, a written request must be filed with the ASCE Managing Editor. The manuscript for this paper was submitted for review and possible publication on December 12, 2006; approved on October 17, 2007. This paper is part of the ***Journal of Hydraulic Engineering***, Vol. 134, No. 6, June 1, 2008. ©ASCE, ISSN 0733-9429/2008/6-784–793/$25.00.

Permeability computation plays an important role in hydrology as flow depends strongly on the nature of the rock heterogeneity. In this domain, the modeling scale [m km] is much larger than the measuring scale (0.01m–0.1m). Therefore, it is of interest to pass from the microstructure obtained by experimental measurements to the macroscopic scale by the homogenization theory.

The reviews of Wen and Gómez-Hernández (1996) and Renard and de Marsily (1997) discuss the different upscaling and homogenization theories currently employed in hydrology. The major difficulty in permeability upscaling lies in the application of correct flow or pressure boundary conditions (BCs) leading to the "intrinsic" permeability tensor. By definition, the "intrinsic" permeability tensor of the window of interest should be a characteristic of the rock structure and therefore independent of the applied boundary conditions. It is important to note that the "intrinsic" permeability tensor might differ from the "so-called" macroscopic permeability. The macroscopic permeability tensor of a media is defined as the result of the upscaling procedure for a given boundary condition. Therefore, the measured macroscopic permeability might differ from the "intrinsic" one if the boundary layers induce numerical errors (see the discussion on the local and global BC below). Another difference might result from the definition of the macroscopic scale. Usually, the macroscopic scale is defined as being the smallest scale for which the upscaling method is meaningful. In other words, the window of interest needs to be larger than the "so-called" representative elementary volume (REV). As we will show in this paper, it is possible to define an "intrinsic" permeability tensor for a given window of interest smaller than the REV. This tensor, however, depends on the location and the size of the window.

White and Horne (1987) developed an upscaling procedure to determine the intrinsic permeability tensor. They assumed two-dimensional Darcian flow behavior on the macroscopic scale, and demonstrated that at least two sets of boundary conditions have to be applied to the borders of the entire rock (aquifer) in order to

determine the parameters of the tensor. Hence, they suggested the use of more than two boundary conditions and to solve the overdetermined system by means of a least squares algorithm in order to minimize the influence of the applied boundary conditions. Pickup et al. (1992) suggested using only two sets of boundary conditions, both corresponding to the flow fields observed in the aquifer of interest. Durlofsky (1991) developed a numerical method allowing the representation of heterogeneities, supposing small scale periodicity in the rock. By applying periodic boundary conditions on the grid block (domain on which the macroscopic permeability is determined) the small scale periodicity of the rock is correctly represented. At the same time, the computation time is reduced as the domain, on which the flow has to be computed, is much smaller than the entire aquifer. The method has been confirmed by Pickup et al. (1994). The procedure proposed by Gómez-Hernández (1990) leads to a substantial reduction of the computation time. Instead of calculating the flow in the entire rock (aquifer), the boundary conditions are applied on a so-called "skin" region situated around the grid block. Thus, the flow is computed on a very small domain. Wen et al. (2000) improved the accuracy of the permeability tensor computation of systems with oriented layering. Using periodic boundary conditions, they suggested a rotation procedure applied to the coordinate system. Pouya and Courtois (2002) and Pouya (2005) proposed a homogenization procedure applied to irregular fractures in rocks. They considered discrete flow in each single fracture and were particularly interested in different boundary condition types. Pouya and Courtois (2002) investigated linear pressure boundary conditions, whereas constant flow conditions were studied in Pouya (2005). Boundary conditions were applied directly on the borders of the averaging window. They concluded that linear pressure drop boundary conditions led to satisfying results.

One can distinguish two major approaches to the application of boundary conditions to compute the intrinsic permeability tensor of a particular grid block. The first, called the "local" method, consists of applying the BC directly at the border of the grid block. The second, the so-called "global" method, consists of applying them at the boundary of the entire domain. On the one hand, the local method has the advantage of strongly reducing the computation time and memory as the equations are only solved inside the block of interest. However, as it has been analytically shown by Wu et al. (2002), the error of the local BC can be important due to the presence of a boundary layer. On the other hand, the global method is less sensitive to the applied BC, but more time (and memory) consuming. For this reason, some authors have developed different procedures to improve the local approach [see the oversampling method proposed by Wu et al. (2002) and the previously mentioned definition of the "skin" region of Gómez-Hernández (1990)]. In the present paper, we will use a global approach.

Another difficulty in upscaling is the determination of the REV. Commonly, by applying correct BC, the REV is obtained by increasing the block of interest until the computed permeability tensor converges. As a consequence, the local method can be more time consuming as the equation has to be recomputed for each block size (instead of only once for the global method).

In the present paper, we will use the following approach based on a global BC method. We generate a sufficiently large network (larger than the REV) to which we apply pressure BC. Then we displace the averaging window (smaller than the network) over the entire network and compute the permeability tensor for each window position. The advantage of this method is that it allows finding the correct size of the REV by investigating the convergence of the permeability but also by its spatial distribution. The global method was selected as the assumption of Poiseuille flow in the individual segments permits the generation of very large networks. Therefore, the boundary condition sensitivity can be reduced and the computational time is less important.

Using this method we investigate network structures consisting of different pore length (segment length) distributions with constant pore throats (segment radius). Additionally, we will show that the method can be applied to anisotropic porous media.

Numerical Network Construction

Often, porous media are modeled by cubic networks (with heterogeneous pore throats). However since the aim of the paper is to investigate two-dimensional networks with heterogeneous pore lengths, our porous model consists of triangles. The method used to construct the network is based on the Delaunay triangulation algorithm. The Delaunay triangulation of a point set in the plane is a set of triangles connecting the points satisfying an "empty circle" property: the circumcircle of each triangle does not contain any of the points. The entire network surface is given by $L \times L$ length unit square. The length unit is defined as the average distance between two nodes. The average node density is thus 1 l^{-2}. Segments have equal radii, with an arbitrary set value equal to $r=10^{-3}$ length units.

Two network types (regular and irregular) have been constructed in order to test the homogenization procedure (see Fig. 1). The networks shown in Fig. 1 consist of a very small number of segments in order to illustrate their structure. The networks used afterwards for the upscaling procedure consist of 2,601 nodes (the network size then becomes $L \times L=51 \times 51$).

Regular networks were obtained by arranging the points at regular distances on the surface. Irregular networks correspond to a random point set. Fig. 2 shows the segment length distribution for both network types. As expected, the regular network consists of only two different segment lengths (the side and the diagonal length of a square). The segment length distribution of the irregular network is more widespread. One can note that by construction, the Delaunay triangulation minimizes the number of long segments, whereas there is no particular limitation to the smallest length. It is also interesting to note that both distributions have nearly the same mean value.

Anisotropic networks were obtained by applying a homothetic transform to the y coordinate of the isotropic regular network ($y'=hy$ with $h\epsilon[0,1]$). Thus, the network height was reduced, whereas the length remained constant (L).

Homogenization Procedure

Poiseuille (laminar) flow is assumed on the level of the individual segment. If the segment length is much larger than its radius, the velocity profile in the center of the segment corresponds to Poiseuille flow, whereas it changes near the entrance and the exit of the segment. We suppose the segments of the present networks to be sufficiently long in comparison to their radius. Thus, the profile change in the nodes can be neglected. Assuming Poiseuille flow in each segment and mass conservation at each node, the linear system describing flow and pressure fields of the entire network are solved as a function of the applied boundary conditions using Gauss algorithm.

Then, an averaging window (size $l \times l$) is passed over the net-

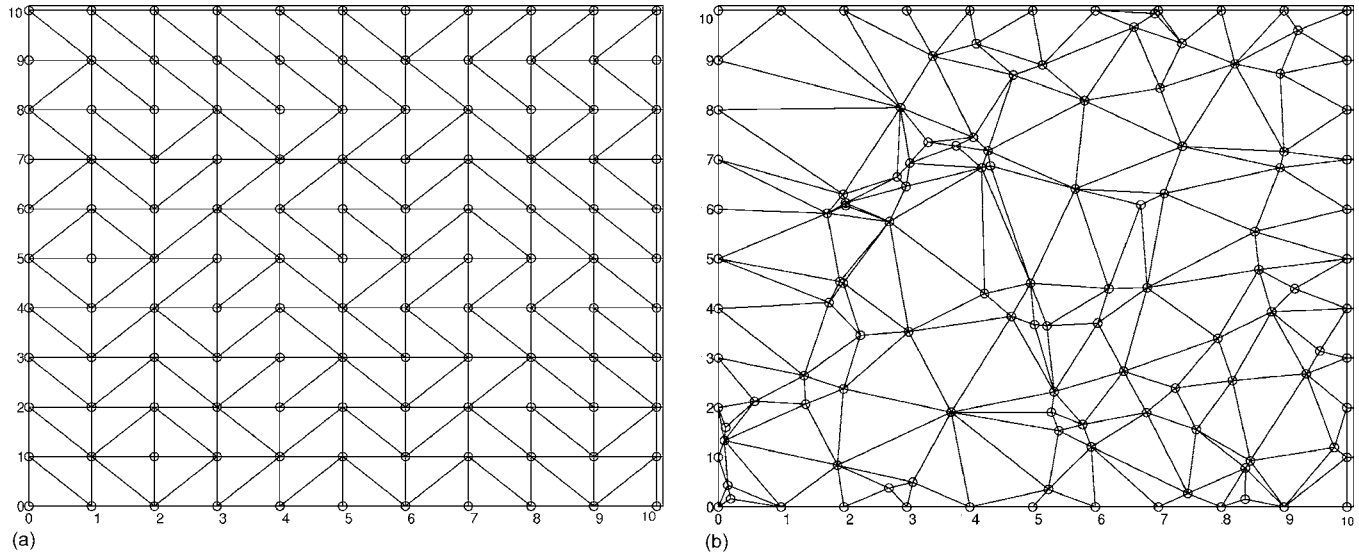

Fig. 1. (a) Regular and (b) irregular network used to compute macroscopic permeability tensor

work structure. The window size is smaller than the total network area (e.g., $l<L$). The objective is then to determine the intrinsic permeability tensor that represents the macroscopic behavior of the window. This means for each window position $\underline{\mathbf{z}}$ there is one permeability tensor describing the mean behavior of the window. It is important to note that the mean properties are computed using the boundary conditions applied to the entire network and not to the averaging window. This permits the computation of the permeability tensor for different window positions by only solving the entire flow and pressure fields twice (see the following paragraph, why twice is sufficient), whereas the so-called local method [see Renard and de Marsily (1997); Wu et al. (2002); Pouya and Courtois (2002); Pouya (2005)] would have required solving the system twice each time the permeability tensor is computed. However, we will recall later that even if the boundary conditions are applied to the network borders, the linear independency of pressure drop conditions permits the determination of the "intrinsic" permeability tensor of the averaging window.

If the averaging window is sufficiently large so that the value of the permeability tensor becomes independent of the window size and its position, the so-called representative elementary volume has been determined.

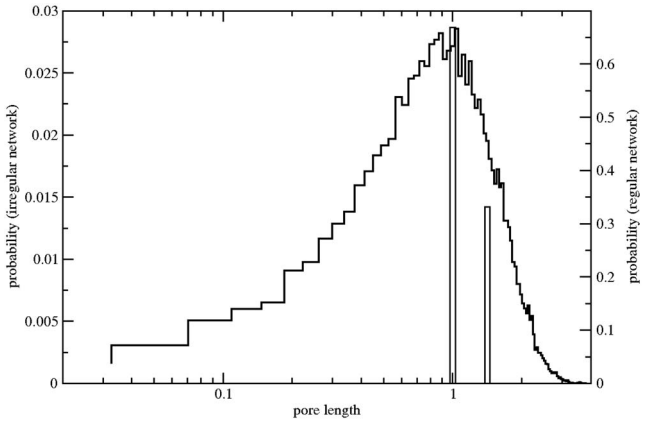

Fig. 2. Pore length probability distribution for irregular (left) and regular (right) network

Obtaining Average Flow Rate and Pressure Gradient

In the following we present the procedure to obtain the average flow rate $\bar{Q}$ and the average pressure gradient $\overline{\nabla P}$ inside the window. We will show that the mean flow and pressure gradient in the averaging window can be obtained using flow and pressure values of the segments of the discrete network crossing the window borders. In this way, the computation becomes easier.

The calculations shown here below are based on Green's formula, which states that for each function $f(\underline{\mathbf{x}})$

$$\int_{\Omega} \operatorname{div} f(\underline{\mathbf{x}}) d\Omega = \int_{\delta\Omega} f(\underline{\mathbf{x}}) \underline{\mathbf{n}}(\underline{\mathbf{x}}) d\sigma \tag{1}$$

where $n(\underline{\mathbf{x}})$=normal vector of the closed surface $\delta\Omega$ over a domain volume Ω.

Average Flow Rate

The average flow rate is given by

$$\bar{Q} = \frac{1}{V_{\text{avg}}} \int_{\Omega} \underline{\mathbf{q}}(\underline{\mathbf{x}}) d\Omega \tag{2}$$

where $\underline{\mathbf{q}}(\underline{\mathbf{x}})$ represents the flow rate at point $\underline{x}$; and V_{avg}=volume of the domain Ω. Using $(\underline{\mathbf{a}} \otimes \underline{\mathbf{b}})_{i,j}=a_i b_j$ and the local mass conservation ($\operatorname{div} \underline{\mathbf{q}}(\underline{\mathbf{x}})=0$), Eq. (2) can be written as

$$\bar{Q} = \frac{1}{V_{\text{avg}}} \int_{\delta\Omega} \operatorname{div}(\underline{\mathbf{x}} \otimes \underline{\mathbf{q}}) d\sigma \tag{3}$$

since

$$\operatorname{div}(\underline{\mathbf{x}} \otimes \underline{\mathbf{q}}) = \underbrace{\operatorname{grad} \underline{\mathbf{x}}}_{\text{unity matrix}} \underline{\mathbf{q}} + \underline{\mathbf{x}} \underbrace{\operatorname{div} \mathbf{q}}_{=0} \tag{4}$$

Hence, using Eq. (1), Eq. (3) becomes

$$\bar{Q} = \frac{1}{V_{\text{avg}}} \int_{\delta\Omega} (\underline{\mathbf{x}} \otimes \underline{\mathbf{q}}) \cdot \underline{\mathbf{n}} \, d\sigma \tag{5}$$

With $(\underline{\mathbf{a}} \otimes \underline{\mathbf{b}})\underline{\mathbf{c}} = \underline{\mathbf{a}}(\underline{\mathbf{b}} \cdot \underline{\mathbf{c}})$ we obtain

$$\bar{Q} = \frac{1}{V_{\text{avg}}} \int_{\delta\Omega} \underline{\mathbf{x}}(\underline{\mathbf{q}} \cdot \underline{\mathbf{n}}) d\sigma \tag{6}$$

In the case of a discrete network, the average flow rate then becomes

$$\bar{Q} = \frac{1}{V_{\text{avg}}} \sum_i \underline{\mathbf{x}}_i (\underline{\mathbf{q}}_i \cdot \underline{\mathbf{n}}) \tag{7}$$

where $\underline{\mathbf{q}}_i$ represents the flow in the segment i crossing the averaging window border.

Average Pressure Gradient

Similarly, the average pressure gradient $\overline{\nabla P}$ is given by

$$\overline{\nabla P} = \frac{1}{V_{\text{avg}}} \int_{\Omega} \nabla P(\underline{\mathbf{x}}) d\Omega \tag{8}$$

where $\nabla P(\underline{\mathbf{x}})$ represents the pressure gradient at point $\underline{\mathbf{x}}$.

Using Eq. (1) $\overline{\nabla P}$ becomes

$$\overline{\nabla P} = \frac{1}{V_{\text{avg}}} \int_{\delta\Omega} P(\underline{\mathbf{x}}) \underline{\mathbf{n}}(\underline{\mathbf{x}}) d\sigma \tag{9}$$

and for a discrete network

$$\overline{\nabla P} = \frac{1}{V_{\text{avg}}} \sum_i \int_{\underline{\mathbf{x}}_i}^{\underline{\mathbf{x}}_{i+1}} P_i(\underline{\mathbf{x}}) \underline{\mathbf{n}} \, dx \tag{10}$$

where the function $P_i(\underline{\mathbf{x}})$ is piecewise defined on the interval $[\underline{\mathbf{x}}_i, \underline{\mathbf{x}}_{i+1}]$ such as

$$P_i(\underline{\mathbf{x}}) = P_i + \frac{\underline{\mathbf{x}} - \underline{\mathbf{x}}_i}{\underline{\mathbf{x}}_{i+1} - \underline{\mathbf{x}}_i} (P_{i+1} - P_i) \tag{11}$$

where P_i (P_{i+1})=pressure at the intersection point $\underline{\mathbf{x}}_i$ (x_{i+1}).

Calculation of Permeability Tensor

In this section, we show how we compute the intrinsic permeability tensor and recall why only two global boundary conditions [in a two-dimensional (2D) network] are sufficient.

Considering a family of boundary conditions depending on two parameters λ_1 and λ_2, for each window position $\bar{Q}$ depends linearly on the local flow field $\underline{\mathbf{q}}(\underline{\mathbf{x}})$ in the network. $\underline{\mathbf{q}}(\underline{\mathbf{x}})$ itself depends linearly on the scalars λ_1 and λ_2. Also, for each window position, the average pressure gradient $\overline{\nabla P}$ depends linearly on the local pressure field $P(\underline{\mathbf{x}})$ itself depending on the scalars λ_1 and λ_2. BC_1 and BC_2=two linearly independent boundary conditions. Thus, $BC=\lambda_1 BC_1+\lambda_2 BC_2$ becomes a boundary condition belonging to this family. Hence, for a certain window position the average flow $\bar{Q}_{BC1}$ ($\bar{Q}_{BC2}$) and the average pressure gradient $\overline{\nabla P}_{BC1}$ ($\overline{\nabla P}_{BC2}$) are given by the boundary condition BC_1 (BC_2). For this window position $\bar{Q}_{BC}$ and $\overline{\nabla P}_{BC}$ given by the boundary condition $BC=\lambda_1 BC_1+\lambda_2 BC_2$ become

$$\bar{Q}_{BC} = \lambda_1 \bar{Q}_{BC1} + \lambda_2 \bar{Q}_{BC2} \tag{12}$$

and

$$\overline{\nabla P}_{BC} = \lambda_1 \overline{\nabla P}_{BC1} + \lambda_2 \overline{\nabla P}_{BC2} \tag{13}$$

Then, we define a matrix $\mathbf{Q}_{BC1,BC2}$ whose columns are given by $\bar{Q}_{BC1}$ and $\bar{Q}_{BC2}$. $\nabla \mathbf{P}_{BC1,BC2}$ corresponds to a matrix given by $\overline{\nabla P}_{BC1}$ and $\overline{\nabla P}_{BC2}$. Thus, the average flow and the average pressure gradient become

$$\bar{Q}_{BC} = \mathbf{Q}_{BC1,BC2} \begin{pmatrix} \lambda_1 \\ \lambda_2 \end{pmatrix} \tag{14}$$

and

$$\overline{\nabla P}_{BC} = \nabla P_{BC1,BC2} \begin{pmatrix} \lambda_1 \\ \lambda_2 \end{pmatrix} \tag{15}$$

Using Eqs. (14) and (15) $\bar{Q}_{BC}$ can be written as

$$\bar{Q}_{BC} = \mathbf{Q}_{BC1,BC2} \nabla P^{-1}_{BC1,BC2} \overline{\nabla P}_{BC} \tag{16}$$

or

$$\mathbf{K}_{BC1,BC2} = \mathbf{Q}_{BC1,BC2} \nabla P^{-1}_{BC1,BC2} \tag{17}$$

$\mathbf{K}_{BC1,BC2}$ is defined as the estimation of the equivalent macroscopic permeability tensor of the averaging window obtained by the boundary conditions BC_1 and BC_2. Thus, two linear independent boundary conditions are sufficient to compute all parameters of the two-dimensional permeability tensor.

Then, we suppose two additional linearly independent boundary conditions BC_3 and BC_4 (which are also independent of BC_1 and BC_2). The resulting estimation of the equivalent macroscopic permeability tensor of the averaging window becomes then $\mathbf{K}_{BC3,BC4}$.

Therefore, we can state, if $\mathbf{K}_{BC1,BC2}$ and $\mathbf{K}_{BC3,BC4}$ are identical then $\mathbf{K}_{BC1,BC2}$ and $\mathbf{K}_{BC3,BC4}$ are equal to the intrinsic permeability tensor $\mathbf{K}$ (if it exists) of the investigated domain (area of the averaging window), $\mathbf{K}$ being independent of the applied boundary conditions. Nevertheless, $\mathbf{K}$ can only be determined if the domain is homogenizable and if the independent boundary conditions BC_1 and BC_2 lead to independent $\bar{Q}_{BC1}$ and $\bar{Q}_{BC2}$ ($\overline{\nabla P}_{BC2}$ and $\overline{\nabla P}_{BC2}$). Thus, using two linear independent boundary conditions applied to the network borders leads to the same results as local methods as long as the average flow and pressure gradient fields inside the window remain linearly independent.

Finally, we computed the parameters of the permeability tensor $\mathbf{K}_{BC1,BC2}$ presented in the Results section by means of Eq. (17).

Results

As a first step, we determine which types of linear independent boundary conditions applied to the network borders lead to linear independent flow and pressure gradient fields inside the averaging window (permitting the determination of the intrinsic permeability tensor) and some examples which do not. Using the correct types of boundary conditions we will then present the principal results, as the representative elementary volume and the ability of the algorithm to deal with anisotropy.

Boundary Conditions

In order to show that the homogenization procedure can provide the intrinsic permeability tensor, different sets of boundary con-

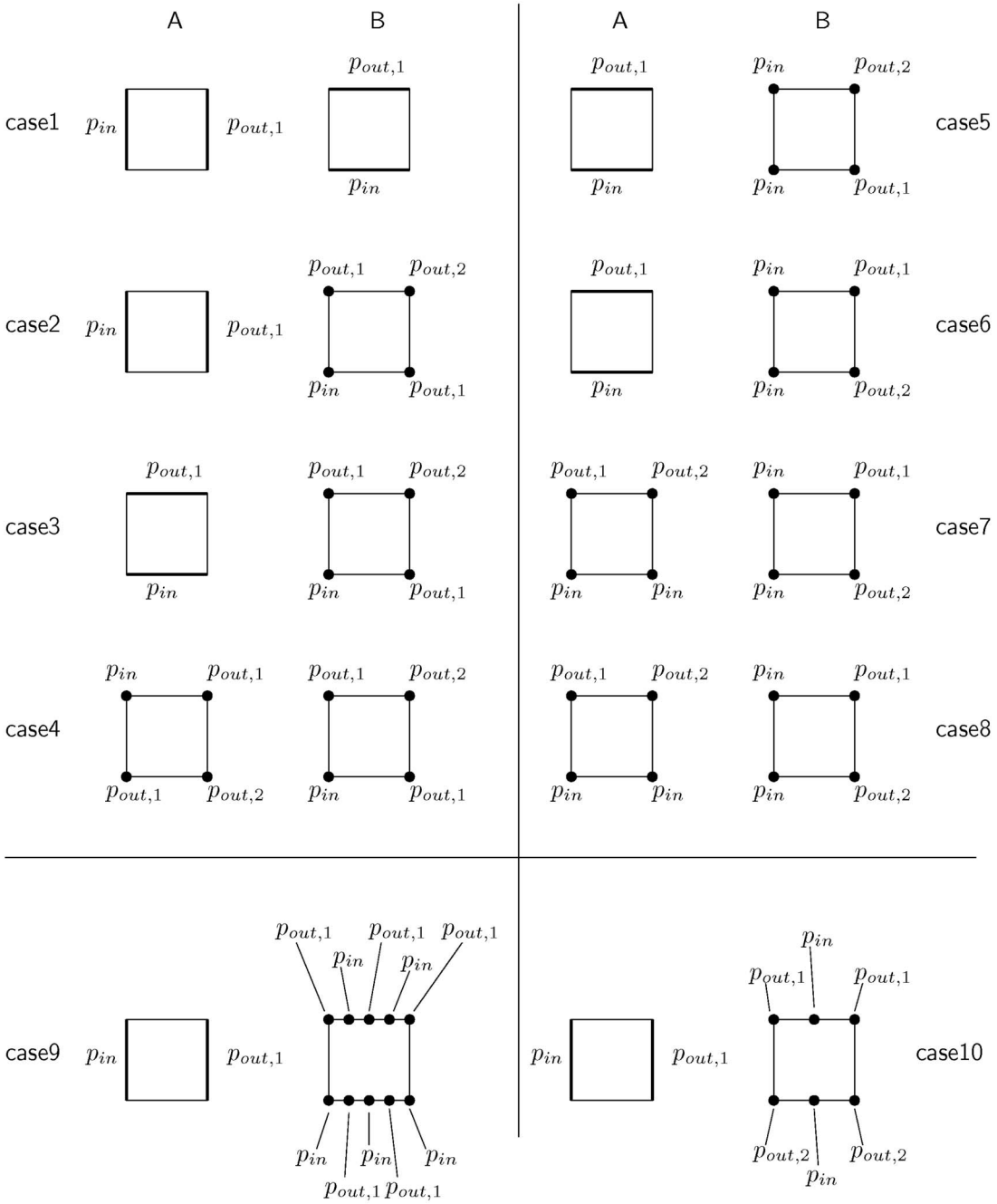

Fig. 3. Applied boundary conditions to test influence of boundary conditions on homogenization result. Bold lines stand for pressure applied on entire corresponding network border. Pressure on thin lines is given by linear relation between pressures given on bold lines or dots ($p_{in} > p_{out,1} > p_{out,2}$).

ditions were applied to the regular isotropic network. The different boundary conditions are shown in Fig. 3. We have tested pressure boundary conditions given by constant pressures or linear pressure drops on the border (Fig. 3, Cases 1–8) and boundary conditions inducing more complex flow and pressure fields (Fig. 3, Cases 9 and 10). Nevertheless, all sets of boundary conditions are linearly independent. Fig. 4 shows the values K_{xx} and K_{yy} as a function of the applied boundary conditions (Case 1–8 of Fig. 3 and for different window positions (window size $l=25$). Since the values of the permeability tensor are relatively independent of the boundary conditions we can conclude that one can compute an intrinsic permeability tensor. Fig. 5 shows the values of K_{xx} and K_{yy} obtained by the boundary conditions corresponding to Cases 9 and 10 of Fig. 3 as a function of the window position. In both cases K_{xx} and K_{yy} strongly depend on the boundary conditions. In those cases, computing the intrinsic permeability tensor is therefore not possible.

In the following, linear pressure drop conditions as shown in Fig. 3 Case 1) will be used.

Representative Elementary Volume

As a first step, it is necessary to determine the REV. The REV stands for the minimal size of the averaging window for which

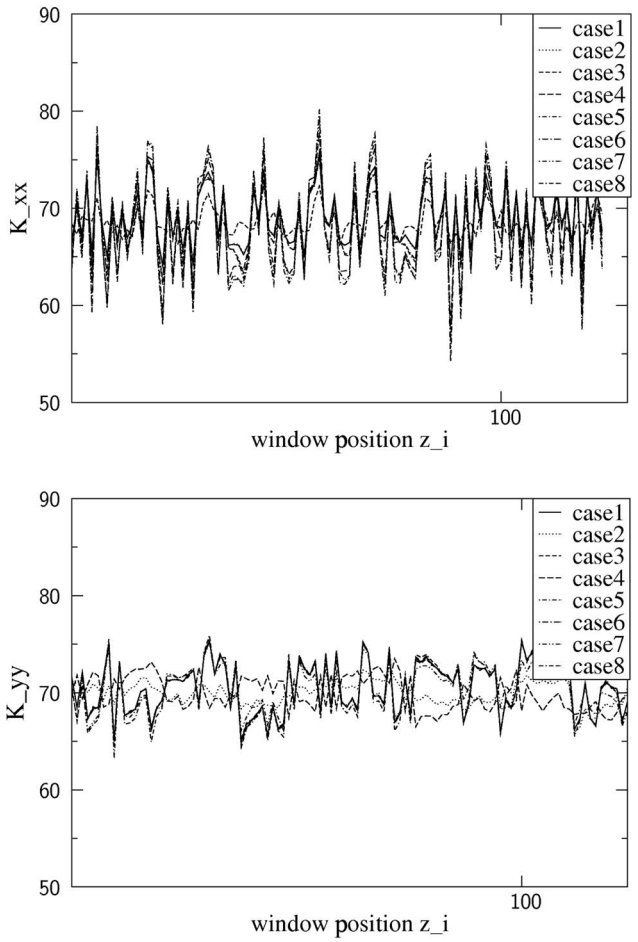

Fig. 4. Values of K_{xx} and K_{yy} of regular isotropic network. Boundary conditions of Cases 1–8 shown in Fig. 3 were applied. Window size is $l=25$.

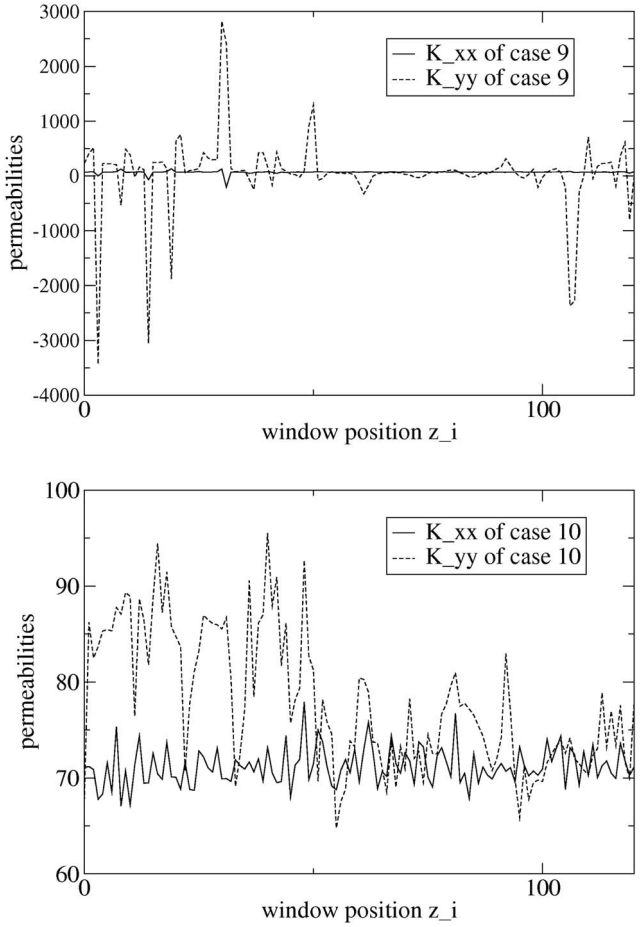

Fig. 5. Values of K_{xx} and K_{yy} of regular isotropic network for different window positions. Boundary conditions correspond to Cases 9 and 10 of Fig. 3. Window size is $l=25$.

values of the permeability tensor become independent of the window size and position (in the case of homogeneous porous media). In the following we only present the results for K_{xx} as the networks are isotropic and $K_{xx}=K_{yy}$.

We now compute the spatial average of the permeability $\langle K_{xx}\rangle$ (where $\langle . \rangle$ denotes a spatial average over all window positions) and its variance. Fig. 6 shows the spatial average and the variance of K_{xx} as the function of the averaging window size. The results correspond to a regular and an irregular network. As expected it can be seen that both (average and variance) decrease with the window size, converging to an asymptotic value. The average value of the regular network converges more rapidly as the small scale fluctuations are less important than in the case of the irregular network. Additionally, one can see that the small scale heterogeneity of the network decreases the global permeability. Similarly, the variance of the regular network converges more rapidly. As expected, the variance of the irregular network is very high for small window sizes.

In the irregular case, it is important to note that the variance converges slower than the average value. Consequently, the variance is more relevant than the average value to characterize the deviation of the current window size to the REV. Therefore, to quantify this deviation (the relative error to the REV) we will introduce the following measurement: $\delta=|\sigma_K/\langle K_{xx}\rangle|$, where σ_K represents the standard deviation of $\langle K_{xx}\rangle$. Using this definition we characterize the rate of convergence on Fig. 7 as the function of the window size. One can note that the regular network converges with the rate $\delta \sim l^{-2}$ and the irregular one with $\delta \sim l^{-1.3}$. These results should to be compared to the analytical results of Wu et al. (2002) proposing a convergence rate of l^{-1}. We thus find a slightly more rapid rate of convergence. Using the results of Fig. 7 we can summarize that the REV size is $l \sim 38$, as above this window size the relative error is smaller than 2.3%.

In the section on Boundary Conditions we have shown that we can still compute an intrinsic permeability tensor, even if the averaging window size $l=25$ is smaller than the REV. This result is particularly interesting as it states that upscaling is still possible in the case of small averaging windows as long as the resulting permeability is spatially heterogeneous. We will now investigate the permeability distribution induced by a window size smaller than the REV. Fig. 8 shows the permeability distribution on a logarithmic scale for a window size of $l=25$ for both the regular and the irregular network. As can been seen on this graph, the distributions fit reasonably well with a log-normal distribution. Again, these results show that, for the same averaging window size, the average value of the regular network is higher. Additionally, the standard deviation is smaller. Comparing the segment length distribution (corresponding to the microscale permeability distribution, Fig. 2) and the permeability distribution (Fig. 8) one can note that the standard deviation is increased by the upscaling procedure. Also, the mean value is changed. Whereas the mean

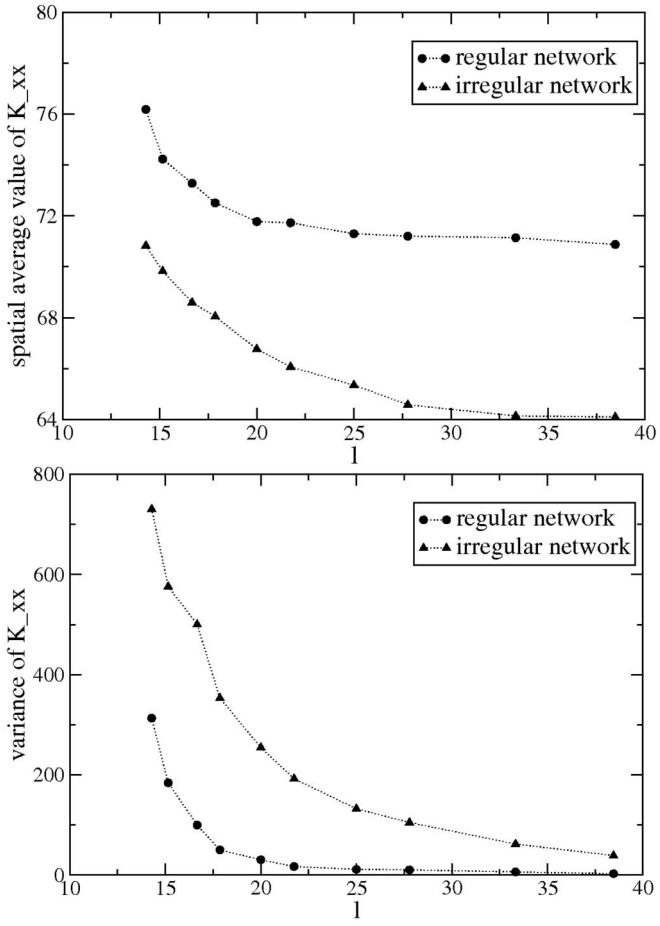

Fig. 6. Spatial average and variance of K_{xx} of regular and irregular network as function of averaging window size l

values of the pore length distribution are the same, the mean value of the permeability of the regular network is significantly higher than the one of the irregular network. This means that the pore structure and connectivity have an important influence on the permeability and should not be neglected by the upscaling procedure.

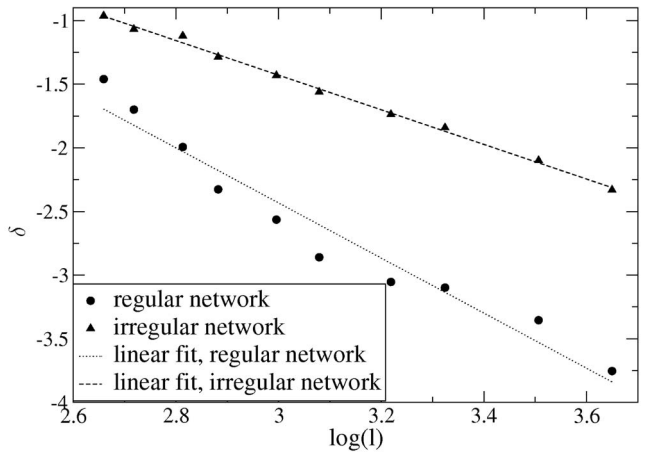

Fig. 7. $\delta = |\sigma_K / \langle K_{xx} \rangle|$ of regular and irregular network as function of averaging window size l

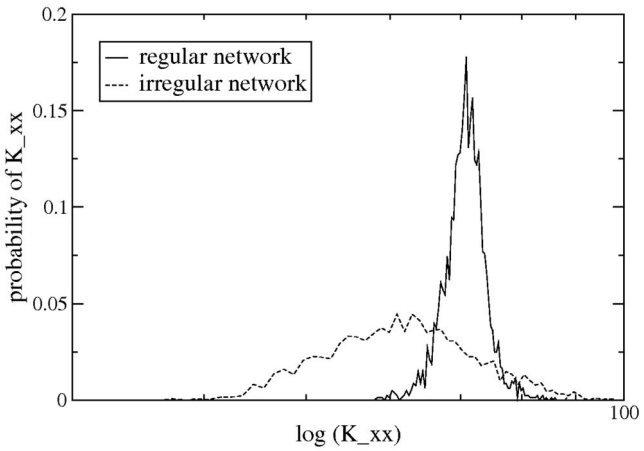

Fig. 8. Probability distribution of K_{xx} of regular and irregular network for averaging window size $l=25$

It is also interesting to characterize the spatial correlation by investigating the covariance function defined as

$$R_{ij}(\boldsymbol{\zeta}) = \langle K_{ij}(\mathbf{z}) K_{ij}(\mathbf{z}+\boldsymbol{\zeta}) \rangle - \langle K_{ij} \rangle^2 \tag{18}$$

Fig. 9 shows the covariance function R_{xx} for different window

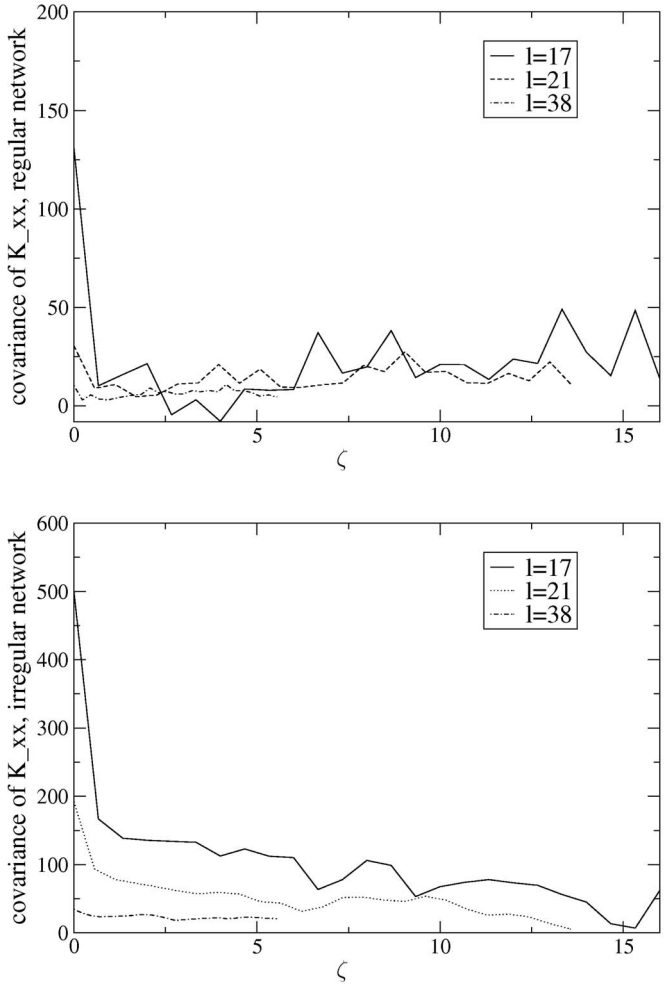

Fig. 9. Covariance of K_{xx} of regular and irregular network as function of averaging window size l

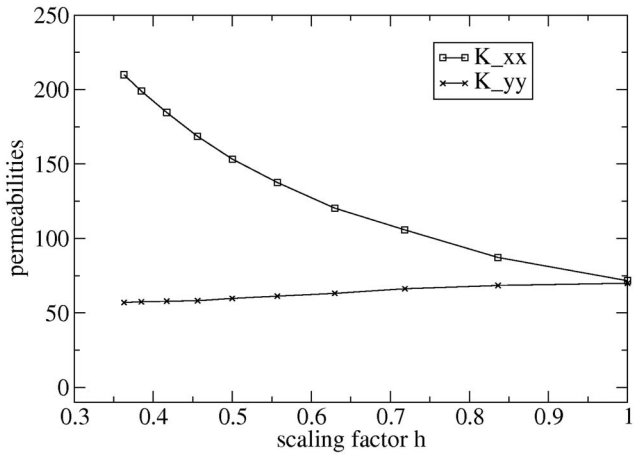

Fig. 10. K_{xx} and K_{yy} of regular anisotropic network as function of scaling factor h

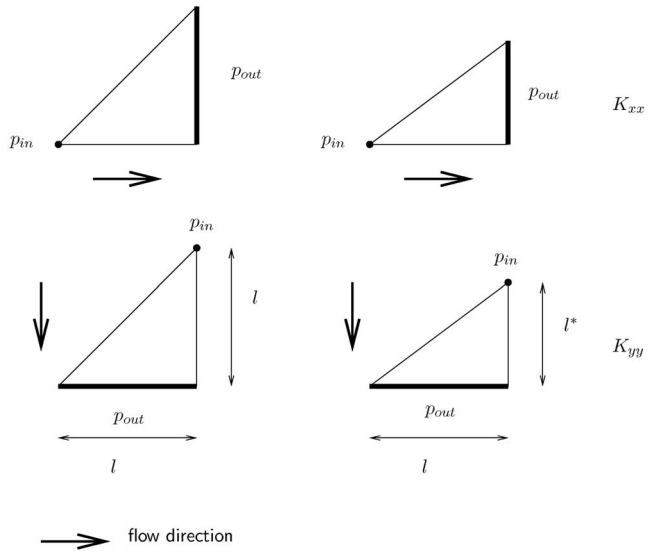

Fig. 11. Networks consisting of three segments to explain dependence of K_{xx} and K_{yy} on scaling factor h. Network length is l, whereas network height after homothetic transform becomes l^*.

sizes for both network types. One can note that for the regular network the correlation length is very small (~ 1) for all window sizes reflecting the fact that microscale spatial variations are on the order of the distance between two nodes. In contrast, the covariance of the irregular network depends strongly on the window size. For small window sizes, the decrease of the covariance is much steeper than for the larger ones.

In this section, we have characterized the REV of our porous model. We have found that the REV size is approximately $l \sim 38$ and shown that, in the case of intermediate window sizes, Darcy's equations are still valid at the macroscopic scale. Nevertheless, a heterogeneous permeability has to be used according to a log-normal distribution. Both the variance and the correlation length depend on the window size. Practically spoken, this means that, if the macroscopic flow field is solved for example using finite differences, in the case of a large window size the permeability is the same for each element, whereas in the case of small window sizes the permeability of each element has to be adapted according to the upscaling procedure.

Permeability values presented above correspond to networks with a constant segment radius set to $r=10^{-3}$ length units. Changing the radius by a factor β ($r'=\beta r$) would lead to an increase in permeability of β^4 (Poiseuilles law is given by $Q \sim r^4/l_0 \Delta P$), whereas the convergence toward the REV (Fig. 7 and the influence of the boundary conditions are not modified. It is nevertheless important to respect the constraints due to Poiseuilles law (segment length $l_0 \gg \beta r$).

Homogenization of Anisotropic Networks

In this section we apply the upscaling procedure to anisotropic networks. The networks were obtained by applying a homothetic transform to the y coordinate of the isotropic regular network ($y'=hy$ with where $h \epsilon [0;1]$ is the scaling factor).

Fig. 10 shows K_{xx} and K_{yy} of the anisotropic network as a function of the scaling factor h. The computation was performed on a regular network. We can note that K_{xx} increases strongly whereas K_{yy} slightly decreases with decreasing system height h. This behavior can be explained by the following analytical reasoning. We consider a network consisting of three segments (see Fig. 11). Boundary conditions were applied as in Case 1 (Fig. 3). The system length is l and the anisotropic system height is $l^*=hl$. By applying the boundary conditions as in Case 1, A, the flow in the x direction can be calculated as

$$Q_x = \frac{\pi r^4}{8\eta}\left(\frac{1}{l} + \frac{1}{\sqrt{l^{*2}+l^2}}\right)\Delta P \tag{19}$$

ΔP=pressure difference ($\Delta P = p_{in} - p_{out}$); r=segment radius; and η=viscosity. In this case, $K_{xx,an}(h)$ (analytical) becomes

$$K_{xx,\mathrm{an}}(h) = \frac{\pi r^4}{8\eta}\left(1 + \frac{1}{\sqrt{\frac{l^{*2}}{l^2}+1}}\right) \tag{20}$$

By applying the boundary conditions as in Case 1, B, the flow in y direction becomes

$$Q_y = \frac{\pi r^4}{8\eta}\left(\frac{1}{l^{*2}} + \frac{1}{\sqrt{l^{*2}+l^2}}\right)\Delta P \tag{21}$$

Thus

$$K_{yy,\mathrm{an}}(h) = \frac{\pi r^4}{8\eta}\left(1 + \frac{1}{\sqrt{\frac{l^2}{l^{*2}}+1}}\right) \tag{22}$$

Eqs. (20) and (22) show that, $K_{xx,\mathrm{an}}(h)$ increases, whereas $K_{yy,\mathrm{an}}(h)$ decreases with decreasing system height (l^*). This is also the case for the numerical permeability values (values obtained by means of the homogenization procedure). In the next step, we compare the analytical and numerical change in permeability.

The numerical values of $K_{xx,\mathrm{num}}(h)$ cannot be directly compared to the analytical values, as we do not consider exactly the same network. The homothetic transform applied to the y coordinate of the network to create anisotropy increases the number of horizontal segments situated in the averaging window. Therefore, if we do not take into account the change in structure of the diagonal segments, we can introduce a parameter $K_{xx,\mathrm{wcs}}(h)$ defined as $K_{xx,\mathrm{wcs}}(h)=K_{xx}(h=1)/h$. Nevertheless, the numerical value of $K_{xx,\mathrm{num}}(h)$ is higher than $K_{xx,\mathrm{wcs}}(h)$. The difference can be explained by the change in structure of the diagonal elements. In

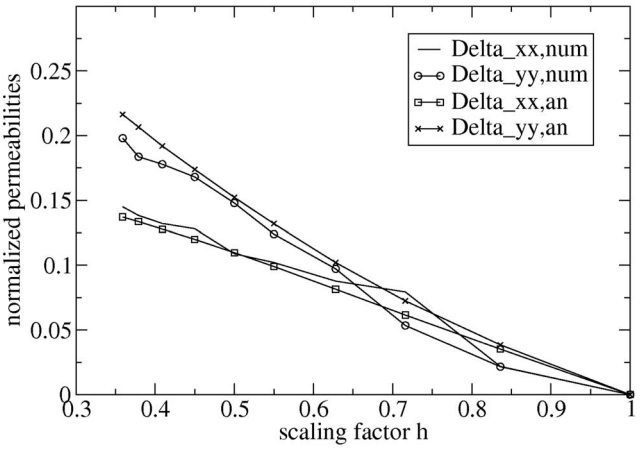

Fig. 12. Analytical and numerical results explaining dependence of K_{xx} and K_{yy} on network anisotropy

order to compare numerical and analytical values, the permeabilities are normalized. Fig. 12 gives the following normalized values

$$\delta_{xx,\mathrm{an}}(h) = \frac{|K_{xx,\mathrm{an}}(h=1) - K_{xx,\mathrm{an}}(h)|}{K_{xx,\mathrm{an}}(h=1)}$$

$$\delta_{yy,\mathrm{an}}(h) = \frac{|K_{yy,\mathrm{an}}(h=1) - K_{yy,\mathrm{an}}(h)|}{K_{yy,\mathrm{an}}(h=1)}$$

$$\delta_{xx,\mathrm{num}}(h) = \frac{|(K_{xx,\mathrm{num}}(h=1) - K_{xx,\mathrm{wcs}}(h=1)) - (K_{xx,\mathrm{num}}(h) - K_{xx,\mathrm{wcs}}(h))|}{K_{xx,\mathrm{num}}(h=1) - K_{xx,\mathrm{wcs}}(h=1)}$$

and

$$\delta_{yy,\mathrm{num}}(h) = \frac{|K_{yy,\mathrm{num}}(h=1) - K_{yy,\mathrm{num}}(h)|}{K_{yy,\mathrm{num}}(h=1)}$$

The results show that the analytical and numerical values are very similar ($\delta_{xx,\mathrm{an}}(h) \approx \delta_{xx,\mathrm{num}}(h)$ and $\delta_{yy,\mathrm{an}}(h) \approx \delta_{yy,\mathrm{num}}(h)$). Hence, the dependence of the anisotropic permeabilities on the system height can be explained by the analytical solution. K_{yy} decreases due to the structure change of the diagonal segments. The increase of K_{xx} is due, on one hand to the higher number of parallel segments and on the other hand to the structure change of the diagonal segments.

Further Comments

The upscaling procedure has been applied to two-dimensional networks. However, it is straightforward to compute the permeability tensor of three-dimensional networks. In this case, three sets of linearly independent boundary conditions have to be applied to the network borders and the REV size has to be recomputed. Convergence to the REV as shown in Fig. 7, is quantitatively the same but the exact value of the convergence rate should also be redetermined.

Additionally, it would be interesting to investigate the behavior of networks close to the percolation threshold, where it is known that the REV size becomes infinite.

With the increasing resolution of X-ray microtomography the reconstruction of the pore structure by so-called pore network models becomes relevant as they give insight into the microscale behavior of the rocks. However, the equivalent macroscopic transport properties still remain important and can be obtained from the reconstructed pore network models using the algorithm presented here. Characterization of the different soil types can then be done in the same way as it was done for the different triangle structures. The relation between the micro- and macroscopic length and permeability distributions as well as the convergence rate toward the REV can than be applied to identify different soil or rock types.

The advantage of this method is its ability to characterize a porous medium even if the upscaling is done with an averaging window smaller than the REV. Indeed, it permits the description of porous media for which the averaging window size is limited by an upper bound. For instance, if the porous medium presents macroscopic variations, the REV size should be larger than the microscopic scale but also smaller than the macroscopic scale. In contrast, classical homogenization procedures require the microscopic and macroscopic scale to be very distant from each other. Otherwise, we have shown that a smaller window size can be applied as long as the induced heterogeneities are taken into account.

We have developed and characterized the present procedure with a well-defined porous model. Future work will consist of investigating systems for which the procedure presents more interest. We particularly plan to study porous media with large scale structure gradients (pore throat, pore length . . .). We also intend to investigate the problem of the interface conditions of two adjacent different porous media [see for instance Beavers and Joseph 1967)]. Indeed, in the neighborhood of the interface, the averaging window size cannot be increased unlimitedly. Thus, our method might be more adapted to deal with such a problem.

Conclusion

In this paper, we used an upscaling procedure based on a global boundary condition method combined with a spatial average. The procedure permits the determination of the REV by computing the entire flow and pressure field only twice. Additionally, it reduces the numerical errors induced by the boundary layers. We applied this method to characterize a porous media model with heterogeneous pore length distribution. The porous media was modeled by triangular networks. We have characterized the REV size corresponding to the network and shown that using window sizes smaller than the REV requires an heterogeneous Darcian description. The permeability has to be distributed according to a log-normal distribution with the variance and the correlation length depending on the window size and the porous microstructure. Finally, we have applied the procedure to an anisotropic regular network for which an analytical solution can be found. We have shown that using the method leads to the correct analytical behavior.

Acknowledgments

This research project has been financed by the Region Ile de France.

References

Beavers, G. S., and Joseph, D. D. (1967). "On the boundary conditions at a naturally permeable wall." *J. Fluid Mech.*, 30, 197–207.

Durlofsky, L. J. (1991). "Numerical calculation of equivalent grid block permeability tensors for heterogeneous porous media." *Water Resour. Res.*, 27, 699–708.

Gómez-Hernández, J. (1990). "Simulation of block permeability conditioned upon data measured at a different scale." *Proc., Model CARE 90: Calibration and Reliability in Groundwater Modelling*, Vol. 195, IAHS, Wallingford, U.K., 407–416.

Pickup, G. E., Jensen, J. L., Ringrose, P. S., and Sorbie, K. S. (1992). "A method for calculating permeability tensors using perturbed boundary conditions." *Proc., 3rd European Conf. on Mathematics of Oil Recovery*, Delft, The Netherlands.

Pickup, G. E., Ringrose, P. S., Jensen, J. L., and Sorbie, K. S. (1994). "Permeability tensors for sedimentary structures." *Math. Geol.*, 26, 227–250.

Pouya, A. (2005). "Tenseurs de permébilité équivalente d'un domaine hétérogène fini." *C. G. Géoscience*, 337, 581–588.

Pouya, A., and Curtois, A. (2002). "Définition de la perméabilité équivalente des massifs fracturés par des méthodes d'homogénéisation." *C. G. Géoscience*, 334, 975–979.

Renard, Ph., and de Marsily, G. (1997). "Calculating equivalent permeability: A review." *Adv. Water Resour.*, 20, 253–278.

Wen, X.-H., Durlofsky, L. J., Lee, S. H., and Edwards, M. G. (2000). "Full tensor upscaling of geologically complex reservoir description." *Proc., 2000 SPE Annual Technical Conf.*, Dallas, SPE No. 62928.

Wen, X.-H., and Gómez-Hernández, J. (1996). "Upscaling hydraulic conductivities in heterogeneous media: An overview." *J. Hydrol.*, 183, 9–32.

White, C. D., and Horne, R. N. (1987). "Computing absolute transmissibility in the presence of fine-scale heterogeneity." *Proc., Symp. on Reservoir Simulation*, San Antonio, Tex., SPE No. 16011.

Wu, X. H., Efendiev, Y., and Hou, T. Y. (2002). "Analysis of upscaling absolute permeability." *Discrete Contin. Dyn. Syst., Ser. B*, 2, 185–204.